Journal of Power Sources 191 (2009) 560–567

Contents lists available at ScienceDirect

Journal of Power Sources

journal homepage: www.elsevier.com/locate/jpowsour

Enhanced methane storage of chemically and physically activated carbide-derived carbon

Sun-Hwa Yeon[a], Sebastian Osswald[a], Yury Gogotsi[a,*], Jonathan P. Singer[b,1], Jason M. Simmons[c], John E. Fischer[b,c], María A. Lillo-Ródenas[d], Ángel Linares-Solano[d]

[a] Department of Materials Science and Engineering and A.J. Drexel Nanotechnology Institute, Drexel University, Philadelphia, PA 19104, USA
[b] Department of Materials Science and Engineering, University of Pennsylvania, Philadelphia, PA 19104, USA
[c] NIST Center for Neutron Research, National Institute of Standards and Technology, Gaithersburg, MD 20899-6102, USA
[d] Departamento de Química Inorgánica, Universidad de Alicante, Ap. correos 99, E-03080, Alicante, Spain

ARTICLE INFO

Article history:
Received 26 December 2008
Received in revised form 7 February 2009
Accepted 9 February 2009
Available online 20 February 2009

Keywords:
Methane storage
Carbide-derived carbon
Small-angle X-ray scattering
Pore size
Activation

ABSTRACT

Carbide-derived carbons (CDCs) produced by chlorination of carbides offer great potential for precise pore size control at the atomic level, making them attractive candidates for energy storage media. CDCs activated with CO_2 or KOH possess distinct improvements in porosity, displaying specific surface areas above 3000 $m^2\ g^{-1}$ and pore volumes above 1.3 $cm^3\ g^{-1}$. These correspond to gravimetric methane uptake of 16 wt% at 35 bar and 25 °C, close to the currently best reported material PCN-14, a metal-organic framework (MOF), at 35 bar and 17 °C or KOH activated anthracite at 35 bar and 25 °C. The best excess gravimetric methane uptake is obtained with a TiC-derived CDC activated with CO_2 at 975 °C for 2 h, namely a very large surface area of 3360 $m^2\ g^{-1}$ resulting in 18.5 wt% at 25 °C and 60 bar. To obtain realistic volumetric methane capacity, the packing density of completely dried CDC was measured, from which we obtain excess capacity of 145 v(STP) v^{-1} from CDC activated with CO_2 at 875 °C for 8 h, 81% of the DOE target (180 v(STP) v^{-1}) at 35 bar and 25 °C. From small-angle X-ray scattering (SAXS) measurements, pore radii of gyration (R_g) between 0.5 nm and 1 nm are determined. Temperature-dependent methane isotherms show that the isosteric heat of adsorption reaches 24 kJ mol^{-1} at the initial stage of low loading.

1. Introduction

Methane has received sustained attention as a future clean energy source due to its natural abundance, relative safety with respect to most other fuels, low cost and low carbon emission. For on-board storage applications in future transportation technologies, additional constraints are placed on proposed material systems, namely high storage capacity, rapid kinetics of storage and release, and efficient cyclability under modest thermodynamic conditions. To compete with gasoline on a large scale, methane storage should exceed the state of the art for related CH_4-based fuels; liquefied natural-gas (LNG) stored at −82 °C at atmospheric pressure, and compressed natural-gas (CNG) at ambient temperature and high pressure, about 200–300 bar [1,2]. Porous materials provide an alternative to satisfying these storage demands. The U.S. Department of Energy (DOE) has set targets for methane uptake at 180 v(STP) v^{-1} (standard temperature and pressure equivalent volume of methane per volume of the adsorbent materials) at 35 bar and ambient temperature [3].

Candidates for achieving these criteria include many forms of carbon and metal-organic framework compounds (MOF), optimized for extremely high specific surface area and specific micropore volumes [3–6], the former generally determined using the Brunauer–Emmett–Teller (BET) analysis of gas sorption isotherms [7]. Recently discovered MOFs provide exceptionally high-surface area (~3000 $m^2\ g^{-1}$) and functionalizable pore walls [3], but as a class, they still suffer from instability of metal ion or hydrogen bonding [8]. Adsorbent natural-gas (ANG) methane storage performance, using activated porous carbons derived from hardwood, coconut shell, or polymers, is comparable to that of CNG at 250 bar [2], with remarkable volumetric methane uptakes ~200 v v^{-1} at 27 °C and pressures between 34 bar and 48 bar [9]. Standard practice in this research is quite naturally to measure methane volumes and storage material masses. For powdered materials, this leads to ambiguities in the conversion from gravimetric (easy to measure) to volumetric uptake (of greater practical interest) since widely diverse sorbent densities are employed to make the conversion, as discussed in detail later.

Carbide-derived carbons (CDCs) possess tunable pore structures and narrow pore size distributions formed through selective

* Corresponding author. Tel.: +1 215 895 6446; fax: +1 215 895 1934.
E-mail address: gogotsi@drexel.edu (Y. Gogotsi).
[1] Present address: Department of Materials Science and Engineering, Massachusetts Institute of Technology, Cambridge, MA 02139, USA.

0378-7753/$ – see front matter © 2009 Elsevier B.V. All rights reserved.
doi:10.1016/j.jpowsour.2009.02.019

etching of crystalline metal carbides. In principle this tuneability implies higher energy densities based on high-surface area with ideal pore size matched to different molecular sizes [10,11]. As-produced TiC-derived carbons show high CH_4 uptake at 1 atm and room temperature [12]. To the best of our knowledge, no high-pressure studies of CH_4 uptake by CDC have been reported. We recently showed that the BET surface area of CDCs can be enhanced by physical or chemical activation, with concomitant improvements in gravimetric capacity for hydrogen from 20% to 50% depending on the choice of CDC and activation chemistry [13].

In this study, we present experimental results concerning the enhancement of methane storage capacity in post-treated activated CDCs, resulting from improved porosity and BET surface area. At 25 °C and 35 bar, the best excess volumetric capacity is obtained with a TiC-derived CDC activated with CO_2 at 875 °C for 8 h, resulting in 145 v(STP) v^{-1} in which the packing density of completely dried CDC was applied for realistic volumetric methane capacity. Correlated experiments were performed to determine the evolution of pore size with different CO_2 treatments, and to learn something about the enthalpy of adsorption/desorption.

2. Experimental

2.1. Sample preparation

Titanium carbide-derived carbon (TiC-CDC) powders were produced by chlorination of TiC powder, particle size 2 μm. This precursor was placed in a horizontal tube furnace, purged in argon flow and heated to temperatures between 400 °C and 1000 °C under flowing chlorine (10–15 cm^3 min^{-1}) for 3 h. TiC-CDC powders chlorinated at 400 °C and 500 °C were then annealed at 600 °C for 2 h under flowing hydrogen to remove residual chlorine and chloride trapped in pores, previous studies showing that this procedure was not necessary at higher chlorination temperatures [12,14]. Physical activation with CO_2 was applied to 600 °C-chlorinated CDC, varying the activation temperature and time at 30–35 cm^3 min^{-1} flow rate. Prior to this, samples were purged for 4 h at ambient temperature in 90 cm^3 min^{-1} CO_2 flow. Chemical activation with KOH using a KOH/CDC ratio of 3 was applied to 800 °C-chlorinated CDC which had first been annealed in NH_3 flow at 600 °C. Similar methods have been applied to TiC-CDC chlorinated from 400 °C to 500 °C with a hydrogen annealing step instead of NH_3 [5,13]. Sample transfer from furnace to measurement apparatus involved brief exposure to air, so all measurements were preceded by a degassing procedure consisting of at least 20 h at 300 °C in 0.2 Torr vacuum, sufficient in our experience to remove adsorbed water and CO_2. Further manipulations, including mass measurement, were performed in a glove box with circulating argon.

2.2. Low-pressure nitrogen and carbon-dioxide sorption measurement

Gas adsorption analysis was performed using Quantachrome Instruments Quadrasorb[2] with N_2 adsorbate at −196 °C and CO_2 at 0 °C. Pore size distributions (PSDs) and pore volumes were determined using the non-local density functional theory (NLDFT) method provided by Quantachrome's data reduction software for N_2 isotherms collected at −196 °C [15]. The NLDFT model assumes slit-shaped pores with uniformly dense carbon walls; the adsorbate is considered as a fluid of hard spheres [15].

2.3. Small-angle X-ray scattering

To obtain a second independent estimate of pore size, small-angle X-ray scattering (SAXS) experiments were performed on a multiangle diffractometer equipped with a Cu rotating anode, double-focusing optics, evacuated flight path, and a two-dimensional wire detector [16]. Powder samples were dried at 80 °C overnight, sealed in 1 mm diameter glass capillaries, and measured in transmission for 30 min. Data were collected over a scattering vector Q range of 0.02–1.60 $Å^{-1}$. An intensity profile from an empty capillary was corrected for X-ray absorption and subtracted from the sample profile.

2.4. High-pressure methane sorption measurement

Methane uptake experiments were performed on a custom-built volumetric Sieverts-type apparatus described in detail elsewhere [17]. The modified-Benedict–Webb–Rubin (MWBR) equation of state was used for analysis of results [18]. The empty cell volume at room temperature was accurately measured. Excess adsorption isotherms were determined by measuring absolute adsorption up to 60 bar, and then subtracting the empty volume contribution using the calculated volume and known system volumes. The gravimetric methane storage capacity in wt% is obtained from grams of methane per 100 g of carbon. Most experiments were performed with the sample at ambient temperature. In one experiment designed to measure the enthalpy of adsorption, the sample was located in a cryostat allowing measurement of six methane isotherms between −73 °C and 25 °C [17].

2.5. Packing density measurement

The packing density of CDCs was determined by pressing 80–100 mg of powder in a cylindrical mold at 2500 kg cm^{-2}. The difference in height of the pin between empty mold and with the compressed sample inside (once the pressure has been released), and the cross-sectional area of 0.34 cm^2, provides a practical density for determining volumetric capacity. The height of the discs obtained was in the range 0.4–0.7 cm. The densities obtained have an estimated error <2%.

3. Results and discussion

3.1. High-pressure methane sorption

Measurements were performed at 25 °C to investigate the methane storage capacity of the CDCs activated by CO_2 or KOH, as shown in Fig. 1. For CO_2 activation, the methane uptake increases with increasing activation time at fixed activation temperature 875 °C (Fig. 1a), and also with increasing activation temperature at fixed activation time of 2 h (Fig. 1b). For CO_2 activation, BET surface area also increases with increasing activation time and temperature (see Table 1). Excess methane adsorption in 600 °C-chlorinated TiC-CDC with 2 h CO_2 activation at 970 °C, reaches 18.5 wt%, at 60 bar and 25 °C methane conditions without saturating, the highest value observed to date for any activated CDC (Fig. 1b, open circles). At the 35 bar DOE target pressure, this is reduced to ∼16 wt%. CO_2 activation above 970 °C leads to the gradual reduction of methane uptake and unacceptably large burnoff (see Table 1) due to small pores coalescing into larger pores. In KOH-activated CDCs (Fig. 1c and d), methane storage capacity increases by 30–40% compared to non-activated or H_2 annealed CDCs.

[2] Certain commercial equipment, instrument, or products are identified to provide a complete description of experimental conditions. Such identification does not imply recommendation or endorsement by NIST.

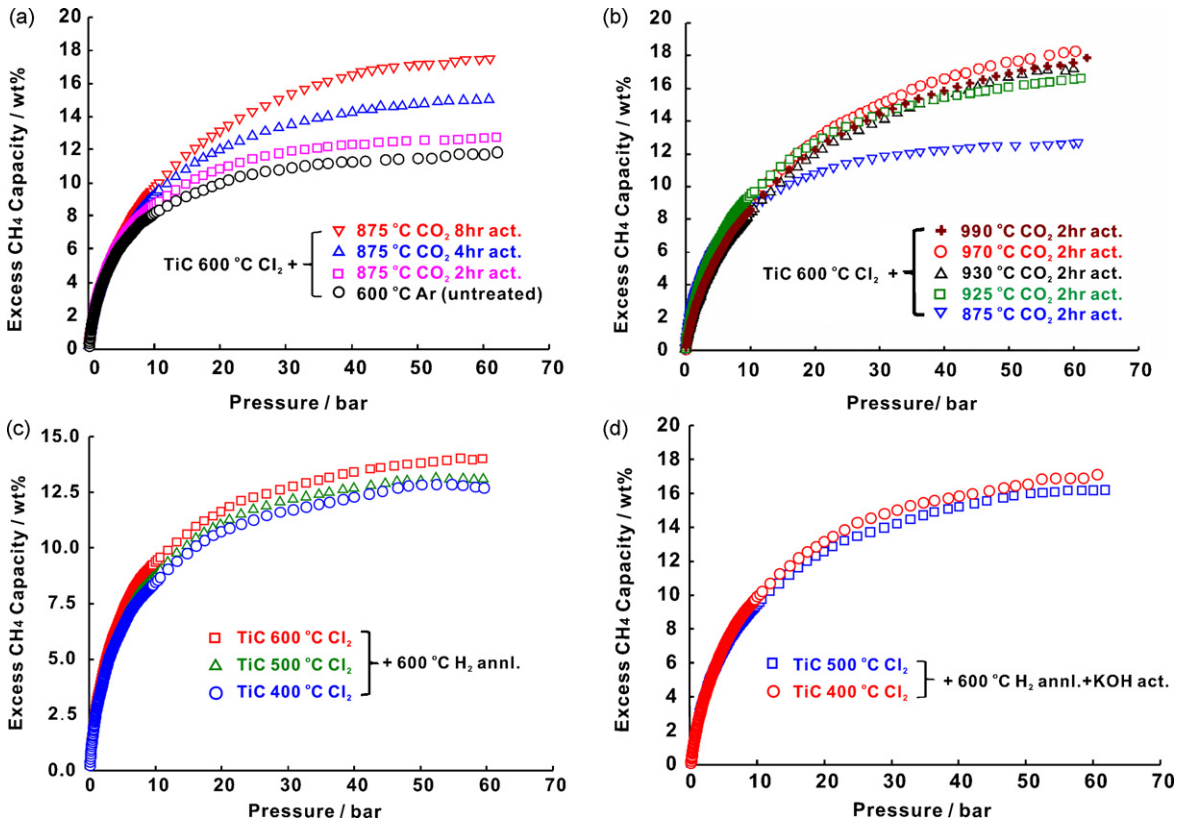

Fig. 1. 25 °C methane excess adsorption isotherms from 0 bar to 60 bar for several TiC-CDCs. (a) CO_2-activated for different times at 875 °C, compared to a control sample heated in argon (open circles); (b) CO_2-activated at different temperatures for 2 h; (c) hydrogen annealed with no activation; and (d) hydrogen annealed followed by KOH activation.

Comparisons of CDC gravimetric and volumetric capacities with examples of state-of-the art MOF (PCN-14 and PCN-11) and activated carbon (KUA31752 and KUA41751) are shown in Fig. 2a and b, respectively. Among CDCs, the highest gravimetric uptake at 25 °C and 35 bar, 16 wt%, is obtained with CO_2 activation at 875 °C for 8 h and 970 °C for 2 h. This is respectively ~20% less than KUA41751 [5,6] and 5% greater than PCN-11 [4]. Also at 35 bar, this highest gravimetric value at 25 °C is only 4–5% less than PCN-14 measured at 17 °C [3] or KOH activated anthracite at 25 °C [5], which are currently the best reported materials. At 60 bar, CO_2 activation for 2 h at 970 °C yields 18.5 wt% gravimetric and 107.5 v v^{-1} volumetric capacities, the latter calculated from the former using the measured packing density of absorbent (discussed below).

Choosing the appropriate density is the crucial factor when evaluating volumetric capacity (v v^{-1}) for methane storage applications [2]. An unrealistic value 220 cm^3(STP) cm^{-3} at 17 °C and 35 bar has been reported for MOFs based on the crystallographic density [3], which amounts to assuming there is no void space in a practical material. CDCs are amorphous, so there is no "crystallographic density"; the ideal *minimum* density is that of the precursor after removal of all non-carbon atoms, with no change in macroscopic volume, 0.98 g cm^{-3} for TiC-CDC [10]. Employing this ideal density in the volumetric conversion yields a value exceeding the DOE target (180 v v^{-1}) by 30% (Fig. 2b). Moreover, this ideal density would only be applicable to bulk CDC produced by chlorinating fully dense ceramic plates such as monolithic TiC ceramic [19]. While only powders have been studied in this work, this number provides a clear indication that porous carbons can outperform MOFs in volumetric methane storage. Taking into account their environmental/thermal stability, environmental safety and cost, they have many advantages over MOFs in energy storage applications.

In practical terms, the most relevant density is the packing density because the amount of adsorbed methane per unit vessel volume depends on the amount of adsorbent loaded into it. Loading a storage tank with void-free polycrystalline adsorbent is not realistic for mass production [5]. Therefore an accurate measurement of adsorbent packing density is necessary. In addition, it is important to thoroughly dry the material before weighing it since adsorbed H_2O and CO_2 will not contribute to methane storage, resulting in overoptimistic volumetric estimates [20]. Also compression does not affect adsorption, nor should it be expected to change the micro/mesopore structure and only minimally affect kinetics [20]. Measurements of CDC packing densities, d_p, are presented in Fig. 3a. Significant powder compaction after CO_2 or KOH activation is achieved. Moreover, the packing density decreases with increasing activation temperature for CO_2 activation. Combined with the gravimetric results, we find the highest value of volumetric methane capacity corresponds to CO_2-activated CDC at 875 °C for 8 h (d_p = 0.61 g cm^{-3}), namely 145 v(STP) v^{-1} at 35 bar and 160 v(STP) v^{-1} at 60 bar.

The decreasing d_p with increasing activation temperature is consistent with increasing weight loss, or burnoff, accompanying the activation process (Table 1). Compared to unactivated CDC, a sharp increase of BET surface area occurs, which can be attributed to the removal of C atoms giving rise to the decreased density. Average pore sizes increase with increasing activation temperature, a finding which is generally true for various carbide precursors processed at high temperatures [10–12]. Fig. 3b and c shows pore size distributions for TiC-CDC annealed in hydrogen and activated by CO_2 and KOH, respectively, determined from sorption data using the NLDFT model for slit pores. While the micropore volume of the unactivated CDC, including the narrow pore size distribution in

Table 1
Characterization results of porous CDC materials by N_2 and CO_2 gas sorption technique.

Cl_2 temperature (°C)	Annealing temperature_time (gas °C_h)	Activation temperature_time (gas °C_h)	BET surface area ($m^2\,g^{-1}$)	Total pore volume ($cm^3\,g^{-1}$)	NLDFT pore volume <1.5 nm (CO_2 ads)[a] ($cm^3\,g^{-1}$)	NLDFT pore volume >1.5 nm (N_2 ads)[a] ($cm^3\,g^{-1}$)	Mean pore width (nm)	Weight loss (%)
600	No	CO_2 875_8	2643	1.05	0.46	0.59	1.49	52
600	No	CO_2 875_4	1911	0.81	0.53	0.28	0.96	27
600	No	CO_2 875_2	1721	0.69	0.54	0.15	0.80	13
600	No	CO_2 925_2	2344	0.96	0.48	0.48	1.35	45
600	No	CO_2 930_2	2409	1.00	0.50	0.5	1.46	51
600	No	CO_2 950_2	3038	1.34	0.42	0.92	1.52	76
600	No	CO_2 970_2	3360	1.30	0.36	0.94	1.80	71
600	No	CO_2 990_2	3300	1.36	0.32	1.04	1.88	72
400	H_2 600_2	KOH	2228	0.90	0.50	0.4	1.2	–
500	H_2 600_2	KOH	1991	0.93	0.49	0.44	1.2	–
400	H_2 600_2	No	1113	0.51	0.49	0.02	0.65	–
500	H_2 600_2	No	1140	0.50	0.48	0.02	0.68	–
600	H_2 600_2	No	1269	0.60	0.58	0.02	0.74	–

[a] These results have been obtained applying the NLDFT method to N_2 and CO_2 adsorption data obtained at −196 °C and 0 °C, respectively.

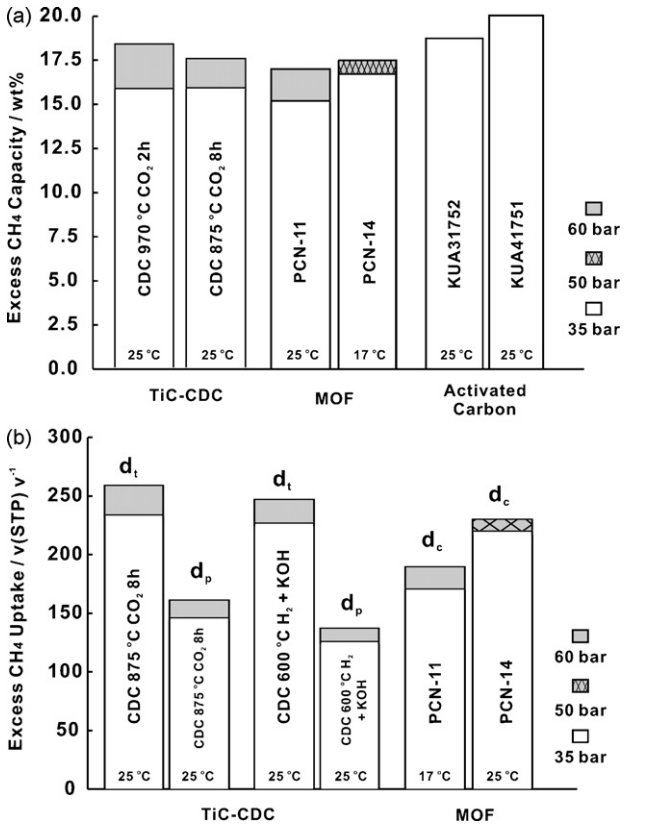

Fig. 2. Comparison of excess (a) gravimetric and (b) volumetric methane capacity for two CDCs, compared with data for a MOF [3,4] and two activated carbons [5,6]. 25 °C and 17 °C measurements at 35 bar (clear), 50 bar (coarse pattern), and 60 bar (shaded) are presented. CDCs were obtained from TiC by 600 °C chlorination for CO_2 activation and 400 °C chlorination for KOH activation. Volumetric results in (b) obtained from gravimetric data (a) using variously the packing (d_p), crystallographic (d_c), and ideal or theoretical (d_t) densities (see text).

the range 0.5–1 nm, was retained after activation, the evolution of pore volume contributed largely to the enhanced methane storage, especially for CO_2 (Fig. 3b).

Our studies of hydrogen storage in CDCs show that gravimetric capacity depends most heavily on the micropore contribution to BET surface area [13,21]. However, theoretical studies of methane storage give an optimum pore size 1.1 nm, in contrast to the optimum for hydrogen 0.58–0.65 nm [22–24]. Here the pore size is the distance between carbon atoms on opposite walls of a slit pore [25,26]. Based on these theoretical studies and porosity results of Table 1, we suggest that activation participates in the formation of additional pores, an advantage for methane storage but probably detrimental for hydrogen storage. However, although CDCs activated by CO_2 possess high BET surface area and high methane uptake by additional mesopore contribution with increasing activation temperature, they have the drawback of low packing density above 930 °C activation temperature, compared to CDCs activated by KOH (Fig. 3).

When we compare the BET surface area between post-activated CDC and KUA41751, the values of specific surface area (SSA) are similar, ~3300–3380 $m^2\,g^{-1}$. However, the pore size distributions are quite different. KUA41751 exhibits a broad Gaussian distribution in the range 0.5–3.0 nm with a mean value ~1.6 nm [6]. On the other hand, post-activated CDC shows both a narrow pore size distribution of micropores 0.5–1.0 nm and a broader distribution of pores. Since the optimum pore size for methane storage is ~1.1 nm, the evolution of pores >1.5 nm in CDCs is responsible for the increase of methane uptake. The methane storage capac-

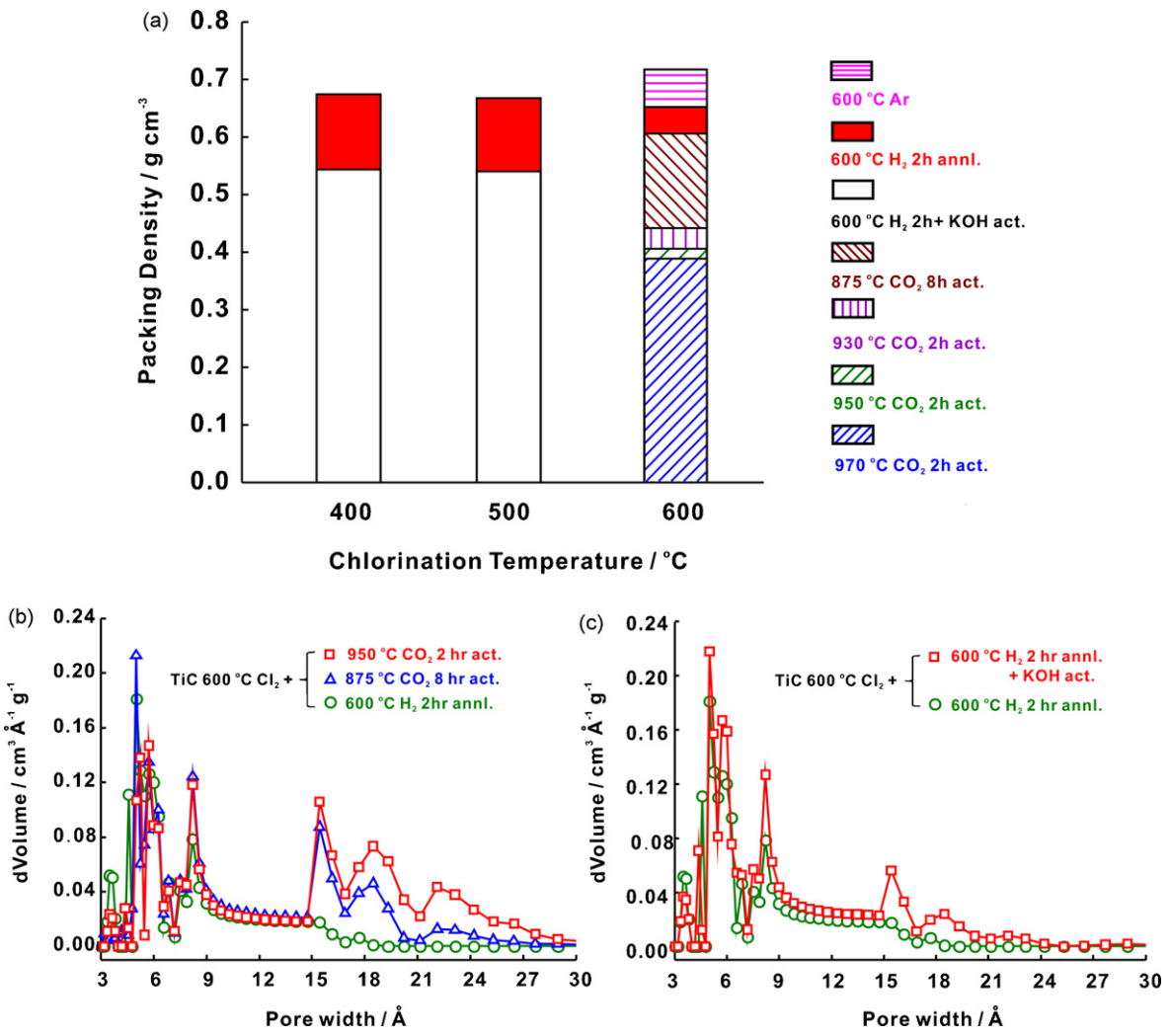

Fig. 3. Experimental packing densities (a) for TiC-CDCs treated by H_2, CO_2 and KOH at the indicated temperatures for 2 h. Pore size distribution obtained for applying NLDFT model to the CO_2 and N_2 sorption data for CDC activated by (b) CO_2 and (c) KOH.

ity of post-treated CDC is somewhat lower than is obtained with the KUA activated carbons, due to a significant portion of micropores. However, in general the distinct pore size distribution in CDC is important for selectivity towards molecules of different sizes.

SAXS measurements were performed on activated CDCs to supplement the information obtained from gas sorption. The SAXS intensity profile $I(Q)$ originates in electron density differences between matrix (carbon) and pores (vacuum), and is insensitive to the connectivity of the pores [27–29]. Fig. 4a and b shows the evolution of TiC-CDC SAXS profiles with CO_2 and KOH activation, respectively. All display the same overall shape, with power law behavior at the lowest Q, a "knee" at intermediate Q and a second power law regime at the highest Q. With CO_2 activation the intermediate "knee" occurs at lower Q compared to the unactivated control sample (inverted triangle and square compared to diamonds); the effect is more subtle with KOH. For both agents the knee becomes broadened with more aggressive activation parameters; with CO_2 the low-Q slope also notably decreases. However, the samples maintain micropores, and increasing the activation temperature has a smaller effect on R_g than increasing the synthesis temperature (Fig. 5a) [30].

These observations can be accounted for quantitatively in terms of different contributions of monodisperse and polydisperse micro- and mesopores. A well-developed knee on a log–log scale signals classic Guinier behavior, Eq. (1), over a narrow Q range, typically ½ decade, for which QR_g is close to unity:

$$I = I_o \exp\left(\frac{-Q^2 R_g^2}{3}\right), \tag{1}$$

where I_o depends on the pore volume and R_g is the pore radius of gyration assuming spheres or ellipsoids of revolution. The high Q limit of the full Guinier expression is the Porod law regime ($I(Q) \propto Q^{-n}$), where n contains information about the pore surfaces (smooth vs. rough, fractal dimension of asperities, etc.). The low-Q limit is a constant I_o if no contrast on length scales larger than R_g is present. None of the profiles in Fig. 4 display this simple behavior, so they must be analyzed in terms of at least two populations. A general approach to this problem was developed by Gibaud et al. [28]:

$$I(Q) = \frac{A}{Q^n} + \frac{B}{(6/R_g^2 + Q^2)} + C, \tag{2}$$

where the first term is the high-Q power law regime of large objects (mesopores, external surfaces of powder grains, etc.) with QR_g below the instrumental cutoff and $n \sim 4$; the second term includes bulk contrast and surface scattering from a population defined by R_g. For a powder of monodisperse pores A is related to the external

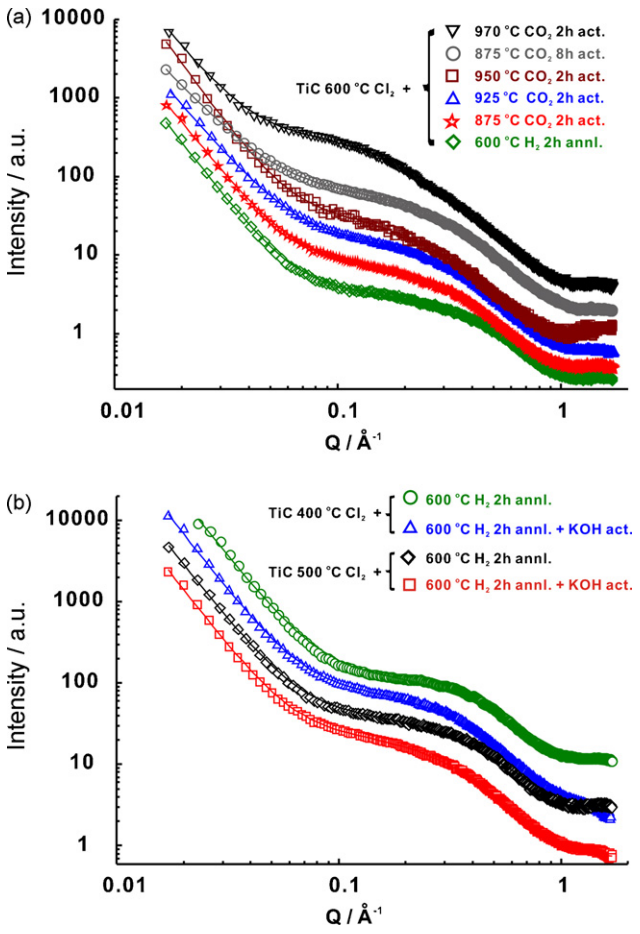

Fig. 4. SAXS profiles from TiC-CDCs activated by CO_2 for the indicated times and temperatures (a); the bottom curve (diamonds) serves as unactivated reference. In (b), the effects of KOH activation on TiC-CDCs chlorinated at 400 °C and 500 °C are compared with unactivated counterparts. These samples were annealed by hydrogen at 600 °C for 2 h prior to KOH activation treatments. Solid lines are best fits to a model consisting of two different populations of contrast objects (see text). Spectra are not normalized so different arbitrary units apply to each intensity profile. Spectra are offset vertically for clarity.

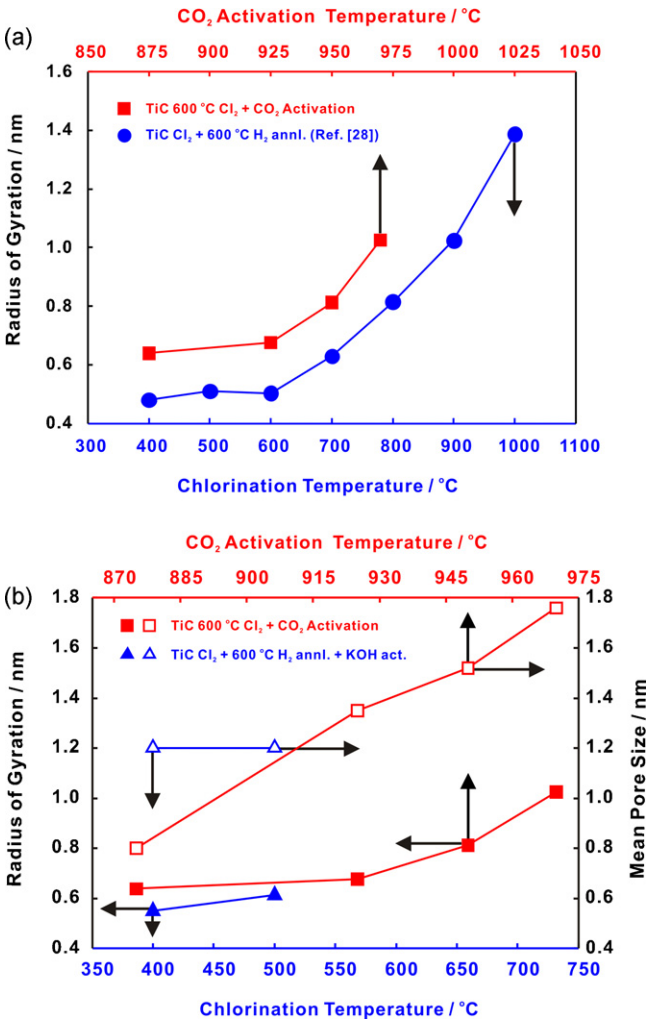

Fig. 5. (a) SAXS-derived radii of gyration (R_g) for TiC-CDCs after the indicated treatments, compared with R_g variation with chlorination temperature [30] and (b) comparison of R_g (filled symbols) with the NLDFT-based mean pore sizes (open symbols) for TiC-CDCs activated by CO_2 gas and KOH.

surface area, B controls the weighting of the defined pore population and C is a constant background. All the profiles can be fitted quite well with this model (solid curves in Fig. 4).

Best fit values of R_g and n are listed in Table 2. For CO_2-activated CDCs, the low-Q exponent n lies between 2.97 with 875 °C activation for 8 h and 3.9 with 950 °C activation for 2 h. The smaller value is attributed to a combination of rough pore wall surfaces and atomic-level disorder [27] introduced into the matrix during activation. The knee is centered in the range $0.25 < Q < 0.5$ Å^{-1} for mild activation conditions (and control samples), but shifts to lower Q ($0.1 < Q < 0.2$; larger "effective" R_g) with CO_2 activation at 950 °C and 970 °C. KOH activation results in increased R_g and no change in n relative to the H_2 annealed control (Fig. 4b). The same applies to R_g variation with chlorination temperature (Fig. 5a and Ref. [30]). In this regard, differences between R_g and mean pore size, 0.5–1.0 nm vs. 0.8–1.6 nm for all samples in this study may be significant. One possible interpretation is the presence of small closed pores which are detected by SAXS but not by gas sorption. However, this is not probable for activated CDC samples. The most probable explanation is that since we have no atomic-scale information on pore shape, the different dimensions could be ascribed to breakdown of assumptions in the two models: perfectly spherical pores in SAXS, slit pores in NLDFT analysis. Although more work is needed to completely understand this relation between SAXS and sorption data, both techniques show that we can control porosity by activation and that the pore size can be more than doubled by activation in CO_2.

To better understand the energetics of adsorption, high-pressure methane isotherms were collected as a function of temperature between −148 °C and 25 °C of TiC-CDC chlorinated at 800 °C followed by annealing in NH_4 at 600 °C (Fig. 6a). TiC-CDC shows increasing methane uptake with decreasing temperature, saturating at 26 wt% at −148 °C (not shown). At room temperature, this CDC adsorbs up to 13.8 wt% at 60 bar. The isosteric heat of adsorption is calculated as a function of methane loading from the isotherms between −73 °C and 25 °C using the Clausius–Clapeyron equation:

$$Q_{st} = R \left. \frac{d(\ln P)}{d(1/T)} \right|_{N_{ads}}. \quad (3)$$

The results of this calculation are shown in Fig. 6b, where the red line is a guide to the eye. At low loading the isosteric heat reaches ~24 kJ mol^{-1}, decreasing to ~18 kJ mol^{-1} at high loadings, indicating that methane begins to fill the lower energy binding sites. This behavior may indicate the heterogonous nature of the activated carbons caused by a wide distribution of pore sizes and surface curvatures [31]. Thus we assign Q_{st} at low coverage to the smaller pores with high-surface curvature. These are quickly saturated with increasing pressure or loading because the high heat of adsorption implies a stronger interaction between neighboring atoms. The low-

Table 2
Comparisons of SAXS-derived radii of gyration and power law exponents for various TiC-CDCs.

Cl_2 temperature (°C)	Annealing temperature_time (gas °C_h)	Activation temperature_time (gas °C_h)	Radius of gyration, R_g (nm)	Power law exponents, n
600	No	CO_2 875_8	0.67	2.97
600	No	CO_2 875_4	0.65	3.65
600	No	CO_2 875_2	0.64	3.53
600	No	CO_2 925_2	0.68	3.28
600	No	CO_2 950_2	0.82	3.90
600	No	CO_2 970_2	1.02	3.48
400	H_2 600_2	KOH	0.55	3.49
500	H_2 600_2	KOH	0.61	3.50
400	H_2 600_2	No	0.46	3.43
500	H_2 600_2	No	0.51	3.44
600	H_2 600_2	No	0.50	3.66

loading Q_{st} is 55% higher than the corresponding value in MOF-5 [17], but is about 20% lower than that measured in PCN-14 [3]. It is very similar to the value 20–24 kJ mol^{-1} for corn grain-derived activated carbon [32]. Although the room temperature uptake of this unactivated CDC is lower than that of the best CO_2-activated CDC, the low-pressure (0–10 bar) isotherms are similar, implying that activation has little effect on the adsorption enthalpy and that increased methane storage capacity is largely due to the increased BET surface area and pore volumes.

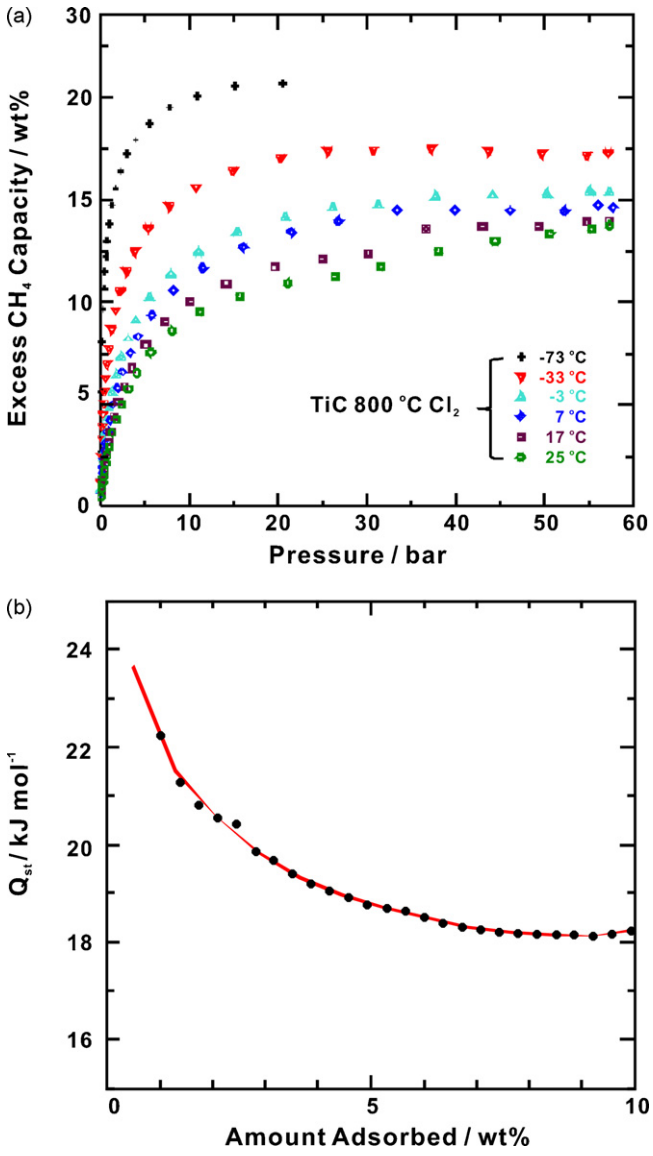

Fig. 6. (a) High-pressure methane excess adsorption isotherm at various temperatures and (b) isosteric heats of adsorption of methane for TiC-CDCs chlorinated at 800 °C and annealed in NH_3 at 600 °C.

4. Conclusions

Through different activation approaches, we showed high uptake of the methane molecules, 18.5 wt% at 25 °C and 60 bar, entrapped in the pores of activated CDC materials with BET surface area of 3360 m^2 g^{-1}. From the pore texture analysis, it is confirmed that the activation of CDC by CO_2 or KOH is efficient to produce activated carbon with the suitable porosity for methane uptake. In volumetric methane uptake, CO_2 activated CDC Exhibits 145 v v^{-1} (81% of the DOE target of 180 v v^{-1} at 25 °C and 35 bar), in which the packing density of completely dried carbon was applied for accurate volumetric conversion. The heat of adsorption of TiC-CDC annealed by NH_3 at 600 °C decreases with increasing gas adsorption, showing strongest biding energy of around ~24 kJ mol^{-1} at the initial stage. Additionally, discrepancies between radius of gyration (R_g) and mean pore size (from NLDFT) in activated CDCs were observed, and explained by deviation of CDC pore shape from slit pores. Thus, the activation of CDCs allows additional control of pore size, shape, and BET surface area for developing storage materials for various gases.

Acknowledgements

We are grateful to Dr. R.K. Dash (Y-Carbon), Dr. H.-S. Kim (Samsung Advanced Institute of Technology), and Dr. C. Portet for experimental help and helpful discussions. This work was supported by the US Department of Energy under EERE grant number DE-FC36-04GO14282. S.Y. was partially supported by the Korea Research Foundation Grant No. KRF-2007-357-D00061 funded by the Korean Government (MOEHRD). J.M.S. acknowledges support from the National Research Council Research Associate Program.

References

[1] R.F. Cracknell, P. Gordon, K.E. Gubbins, J. Phys. Chem. 97 (1993) 494–499.
[2] J. Wegrzyn, M. Gurevich, Appl. Energy 55 (1996) 71–83.
[3] S. Ma, D. Sun, J.M. Simmons, C.D. Collier, D. Yuan, H.-C. Zhou, J. Am. Chem. Soc. 130 (2008) 1012–1016.
[4] X.-S. Wang, S. Ma, K. Rauch, J.M. Simmons, D. Yuan, X. Wang, T. Yildirim, W.C. Cole, J.J. Lopez, A. Meijere, H.-C. Zhou, Chem. Mater. 20 (2008) 3145–3152.
[5] D. Lozano-Castello, D. Cazorla-Amoros, A. Linares-Solano, Energy Fuel 16 (2002) 1321–1328.
[6] D. Lozano-Castell, J. Alcaniz-Monge, M.A. de la Casa-Lillo, D. Cazorla-Amor, A. Linares-Solano, Fuel 81 (2002) 1777–1803.
[7] F. Stoeckli, T.A. Centeno, Carbon 43 (2005) 1184–1190.
[8] M. Sabo, A. Henschel, H. Frode, E. Klemm, S. Kaskel, J. Mater. Chem. 17 (2007) 3827–3832.
[9] P. Pfeifer, J.W. Burress, M.B. Wood, C.M. Lapilli, S.A. Barker, J.S. Pobst, R.J. Cepel, C. Wexler, P.S. Shah, M.J. Gordon, G.J. Suppes, S.P. Buckley, D.J. Radke, J. Ilavsky, A.C. Dillon, P.A. Parilla, M. Benham, M.W. Roth, MRS Conf. Proc. 1041 (2007), R02-02.

[10] Y. Gogotsi, A. Nikitin, H. Ye, W. Zhou, J.E. Fischer, B. Yi, H.C. Foley, M.W. Barsoum, Nat. Mater. 2 (2003) 591–594.
[11] J. Chmiola, G. Yushin, R. Dash, Y. Gogotsi, J. Power Sources 158 (2006) 765–772.
[12] R. Dash, J. Chmiola, G. Yushin, Y. Gogotsi, G. Laudisio, J.P. Singer, J.E. Fischer, S. Kucheyev, Carbon 44 (2006) 2489–2497.
[13] Y. Gogotsi, C. Portet, S. Osswald, T. Yildirim, G. Laudisio, J.E. Fischer, Int. J. Hydrogen Energy, in press.
[14] J. Chmiola, G. Yushin, Y. Gogotsi, C. Portet, P. Simon, P.L. Taberna, Science 313 (2006) 1760–1763.
[15] P.I. Ravikovitch, A.V. Neimark, Colloids Surf. A 187–188 (2001) 11–21.
[16] Multi-angle X-ray Scattering. http://www.irsm.upenn.edu/lrsm/facMAXS.html.
[17] W. Zhou, H. Wu, M.R. Hartman, T. Yildirim, J. Phys. Chem. C 111 (2007) 16131–16137.
[18] NIST Standard Reference Database, 23: NIST Reference Fluid Thermodynamic and Transport Properties Database.
[19] D.A. Ersoy, M.J. McNallan, Y. Gogotsi, Mater. Res. Innov. 5 (2001) 55–62.
[20] J.P. Singer, A. Mayergoyz, C. Portet, E. Schneider, Y. Gogotsi, J.E. Fischer, Micropor. Mesopor. Mater. 116 (2008) 469–472.
[21] G. Yushin, R. Dash, J. Jagiello, J.E. Fischer, Y. Gogotsi, Adv. Funct. Mater. 16 (2006) 2288–2293.
[22] Q. Wang, J.K. Johnson, J. Chem. Phys. 110 (1999) 577–586.
[23] M. Rzepka, P. Lamp, M.A. de la Casa-Lillo, J. Phys. Chem. B 102 (1998) 10894–10898.
[24] I. Cabria, M.J. Lopez, J.A. Alonso, Phys. Rev. B 78 (2008) 075415.
[25] K.R. Matranga, A.L. Myers, E.D. Glandt, Chem. Eng. Sci. 47 (1992) 1569–1579.
[26] P.N. Aukett, N. Quirke, S. Riddiford, S.R. Tennison, Carbon 30 (1992) 913–924.
[27] A. Hasmy, E. Anglaret, M. Foret, J. Pelous, R. Jullien, Phys. Rev. B 50 (1994) 6006.
[28] A. Gibaud, J.S. Xue, J.R. Dahn, Carbon 34 (1996) 499–503.
[29] D. Cazorla-AmorÓs, C.S.-M. de Lecea, J. Alcañiz-Monge, M. Gardner, A. North, J. Dore, Carbon 36 (1998) 309–312.
[30] G. Laudisio, R.K. Dash, J.P. Singer, G. Yushin, Y. Gogotsi, J.E. Fischer, Langmuir 22 (2006) 8945–8950.
[31] I.A.A.C. Esteves, M.S.S. Lopes, P.M.C. Nunes, J.P.B. Mota, Sep. Purif. Technol. 62 (2008) 281–296.
[32] M.S. Balathanigaimani, W.-G. Shim, J.-W. Lee, H. Moon, Micropor. Mesopor. Mater. 119 (2009) 47–52.